Nanoscale

Accepted Manuscript

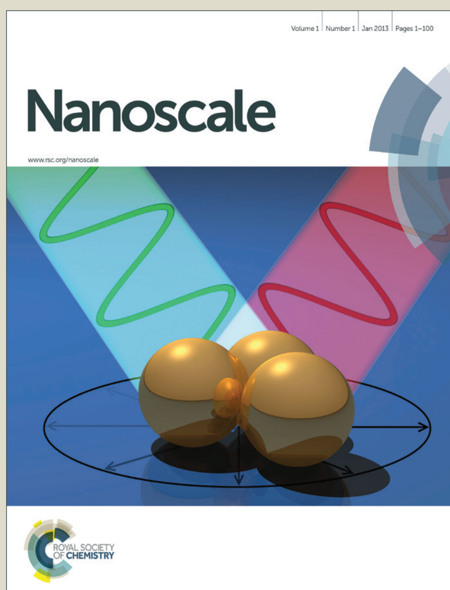

This is an *Accepted Manuscript*, which has been through the Royal Society of Chemistry peer review process and has been accepted for publication.

Accepted Manuscripts are published online shortly after acceptance, before technical editing, formatting and proof reading. Using this free service, authors can make their results available to the community, in citable form, before we publish the edited article. We will replace this *Accepted Manuscript* with the edited and formatted *Advance Article* as soon as it is available.

You can find more information about *Accepted Manuscripts* in the Information for Authors.

Please note that technical editing may introduce minor changes to the text and/or graphics, which may alter content. The journal's standard Terms & Conditions and the Ethical guidelines still apply. In no event shall the Royal Society of Chemistry be held responsible for any errors or omissions in this *Accepted Manuscript* or any consequences arising from the use of any information it contains.

ROYAL SOCIETY OF CHEMISTRY

www.rsc.org/nanoscale

Nanoscale

Nanoscale

Dynamic Article Links ►

Cite this: DOI: 10.1039/c0xx00000x

www.rsc.org/xxxxxx

ARTICLE TYPE

Neutron Diffraction as a Precise and Reliable Method for Obtaining Structural Properties of Bulk Quantities of Graphene

Zdeněk Sofer*[a], Petr Šimek[a], Ondřej Jankovský[a], David Sedmidubský[a], Přemysl Beran[b] and Martin Pumera[c]

Received (in XXX, XXX) Xth XXXXXXXXX 20XX, Accepted Xth XXXXXXXXX 20XX
DOI: 10.1039/b000000x

The graphene based carbon materials have attracted great deal of attention in the last decade; nowadays tons of graphene are produced yearly. However, there is lack of precise and reliable techniques for determination of structural properties of graphene in bulk scales. The analytical methods being routinely applied for graphene characterization, including TEM and AFM can be only used for the study of scant parts of graphene samples and do not give general information on the average number of layers and structure of the prepared graphenes. On the other hand, diffraction methods can be advantageously used to obtain information on average thickness of produced graphene as well as on average sheets lateral dimensions, without the necessity of sample dispersion in solvent. We present a study of the structural properties of graphene prepared by chemical and thermal reduction of graphite oxide, comparing SEM, STEM, AFM, Raman spectroscopy, BET, X-ray and neutron diffraction methods. Our study brings new deep insight into the basic structural properties of graphene in a bulk form. Given the importance of proper characterization technique on the bulk materials, we wish to highlight the importance of these diffraction techniques for accurate determination of the graphene thickness and lateral parameters.

Introduction

Graphene is one of the most intensively studied materials since its discovery in 2004 due to its unique physical, chemical, mechanical and electronic properties.[1] The ballistic transport of free charge carriers and high electrical conductivity gives big prospects for future potential applications of graphene such as transparent electrodes, solar cells, display devices, electrochemical and biochemical sensors, energy and halogen storage and graphene-based composites.[2-7]

The synthesis of graphene is based on the top-down or bottom-up procedures. Bottom-up methods are usually based on a CVD deposition of carbon on metallic substrates. CVD techniques yield graphene with sufficient quality for microelectronic devices.[8] The main advantage of top-down methods is the possibility of a large scale production of graphene. They can be divided into two branches: (i) the mechanical exfoliation of graphite and (ii) the two step method of the oxidation of graphite followed by reduction of the formed graphite oxide. For the purpose of graphite oxidation, mixtures of concentrated acids, such as nitric and sulfuric acid, are used in combination with strong oxidizing agents like potassium permanganate and potassium chlorate.[9-11]

Graphite oxide can be reduced to graphene by thermal or chemical reduction. Graphite oxide undergoes thermal reduction at temperatures over ~200 °C if high heating rate is applied. Functional groups (hydroxyl, epoxide and carboxyl groups) on graphite oxide decompose to form gaseous products, such as CO, CO_2, H_2O and various organic compounds.[12] The gases formed in between the layers of graphite oxide cause an extreme increase of the interlayer pressure which eventually leads to exfoliation. Compared to thermal reduction, chemical reduction of graphite oxide is usually performed at mild conditions so that lower concentration of defects is observed within graphite oxide. Chemical reduction is also much more suitable for fabrication of highly conductive materials like conductive plastics, inks and ceramics. Recently, hydrogen sulphide,[13] hydrazine,[14] sodium borohydride,[15] or lithium aluminium hydride,[16] have been used for chemical reductions.[17] Also reduction by the active hydrogen, which was formed by dissolving of metal in acid environment, has been reported.[18-20]

Structure of graphene has been successfully characterized using various microscopic methods. These include AFM, TEM, SEM, or Raman microscopy.[21-24] It should be highlighted that microscopic techniques provide knowledge about very small amount of the sample and this knowledge is impossible to be extrapolated to bulk amount of samples. For an example single layer and few-layer graphene sheets were analysed by HRTEM and electron diffraction.[21] Pioneering structural characterization by X-ray diffraction was done by Wang *et al.*[25] and structural defects in graphene were analysed and described by Banhart *et al.*[26]

In this contribution, we wish to demonstrate that X-ray

Nanoscale Accepted Manuscript

diffraction and neutron diffraction can provide precise information on the structural properties of graphene prepared by both chemical and thermal reduction; far superior to microscopic techniques (SEM, TEM, AFM) or BET and Raman spectroscopy for bulk amounts of the sample.

Experimental section

Graphite oxide was prepared according to Hofmann method from graphite (99.9%, Fluka, Switzerland). Sulfuric acid (98 %), nitric acid (68 %), potassium chlorate (> 99%), hydrochloric acid (37%), silver nitrate (> 99.8%), barium nitrate (> 99%), hydrazine hydrate (99%), potassium hydroxide and methanol (> 99.9%) were obtained from Penta, Czech Republic. Deionized water (16.8 MΩ) was used for buffer preparation. Hydrogen (99.9999% purity) and nitrogen (99.9999% purity) was obtained from SIAD, Czech Republic.

Graphite oxide prepared according to the Hofmann method was termed as HO-GO. Concentrated sulphuric acid (87.5 mL) and nitric acid (27 mL) were added to a reaction flask containing a magnetic stir bar. The mixture was then cooled to 0°C, and graphite (5 g) was added. The mixture was vigorously stirred to avoid agglomeration and to obtain a homogeneous dispersion. While keeping the reaction flask at 0°C, potassium chlorate (55 g) was slowly added to the mixture. Upon the complete dissolution of the potassium chlorate, the reaction flask was then loosely capped to allow the escape of the evolved gas and the mixture was continuously vigorously stirred for 96 h at room temperature. After completion of the reaction, the mixture was poured into deionized water (3 L) and decanted. The graphite oxide was first redispersed in HCl (5%) solution to remove sulphate ions and then repeatedly centrifuged and redispersed in deionized water until all chloride and sulphate ions were removed. The graphite oxide slurry was then dried in a vacuum oven at 50°C for 48 h.

Thermally reduced graphene denoted as "TRG" was prepared in a quartz glass reactor. 0.5 g of graphite oxide was placed inside the reactor and flushed three times with nitrogen. The reactor was inserted into the hot zone of the furnace preheated to 900°C. The exfoliation of HO-GO was performed in a flow of nitrogen (500 $mL.min^{-1}$) for 3 minutes in order to remove the byproducts of the exfoliation. After exfoliation, the reactor was removed from the furnace hot zone and cooled to room temperature under nitrogen atmosphere. Extremely voluminous TRG was wetted with methanol and dried for 48 hours in a vacuum oven. By this procedure, volume of the TRG is reduced more than ten times. Subsequently, the reduced graphene was heated in a nitrogen/hydrogen atmosphere (500 $mL.min^{-1}$ N_2 and 500 $mL.min^{-1}$ H_2). For this procedure, graphene was placed in a quartz glass reactor and inserted into the furnace preheated to 900 °C for 30 minutes. Then, graphene was cooled to room temperature in a nitrogen/hydrogen atmosphere.

Chemically reduced graphene denoted as "CRG" was prepared by a reduction with hydrazine hydrate. 1 g of graphite oxide was dispersed in 1 L of deionized water by ultrasonication (150 W, 60 minutes). The suspension was alkalized to pH 10 by 1 M KOH. 10 ml of hydrazine hydrate was added to the reaction mixture and the solution was kept under reflux for 24 hours. The obtained CRG was separated from the reaction mixture by suction filtration using a nylon membrane with 0.45 μm porosity. To remove the rest of the reaction products, graphene was repeatedly washed with deionized water and methanol. Prior to further use, the CRG was dried in a vacuum oven at 60 °C for 48 hours.

Combustible elemental analysis (CHNS-O) was performed with a *PE 2400 Series II CHNS/O Analyzer* (Perkin Elmer, USA). In CHN operating mode, the most robust and interference free mode, the instrument employs a classical combustion principle to convert the sample elements to simple gases (CO_2, H_2O and N_2). The PE 2400 analyzer automatically performs combustion, reduction, homogenization, separation and detection of the gases. An MX5 (Mettler Toledo) microbalance was used for precise sample weighing (1.5 – 2.5 mg per single sample analysis). The accuracy of CHN determination is better than 0.30 abs.% Internal calibration was performed using N-phenyl urea.

High resolution X-ray photoelectron spectroscopy (XPS) was performed on an *ESCAProbeP* (Omicron Nanotechnology Ltd, Germany) spectrometer equipped with a monochromatic aluminum X-ray radiation source (1486.7 eV). A wide-scan survey with subsequent high-resolution scans of the C 1s core level of all elements was performed. The relative sensitivity factors were used in the evaluation of the carbon-to-oxygen (C/O) ratios from the survey spectra. Samples were attached to a conductive carrier made from high purity silver bar.

An *inVia Raman microscope* (Renishaw, England) with a CCD detector was used for Raman spectroscopy in backscattering geometry. A Nd-YAG laser (532 nm, 50 mW) with 50x magnification objective was used for measurements. Instrument calibration was performed with a silicon reference which gives a peak centre at 520 cm^{-1} and a resolution of less than 1 cm^{-1}. In order to avoid radiation damage, laser power output used for this measurement was kept in a range of 0.5 mW to 25 mW. Prior to measurements, the samples were suspended in deionized water (concentration 1 mg/ml) and ultrasonicated for 5 minutes. Then the suspension was deposited on a small piece of silicon wafer and dried.

All samples were analysed by X-ray powder diffraction (XRD). Data collection was done with a *PANalytical X'Pert PRO* diffractometer in Bragg–Brentano parafocusing geometry. A CuK_α radiation was used. Diffraction pattern were collected between 5° and 80° of 2θ. The obtained data were refined using Rietveld method.

For the measurement of Atomic Force Microscopy (AFM) images, the samples were suspended in isopropanol (1 mg/ml) and ultrasonicated for 15 minutes (75 W). After sedimentation, the suspension of graphene was dropped on a freshly cleaved mica substrate. These measurements were carried out on an Ntegra Spectra from NT-MDT. The surface scans were performed in a tapping (semi-contact) mode. Cantilevers with a strain constant of 1.5 $kN.m^{-1}$ equipped with a standard silicon tip with curvature radius lower than 10 nm was used for all measurements.

Graphene was investigated by Scanning electron microscopy (SEM) using a Tescan Lyra dual beam microscope with an FEG electron source with an accelerating voltage of 10 kV. Transmission electron microscopy using scanning transmission electron (STEM) detector was performed on a Tescan Lyra dual

Nanoscale Accepted Manuscript

This journal is © The Royal Society of Chemistry [year]

beam microscope. 30 kV accelerating voltage was used for observations. A suspension of graphene with isopropanol (1 mg/ml) was ultrasonicated for 15 minutes (75 W) before use. The bright field modes were used for imaging.

Neutron powder diffraction was performed on instrument MEREDIT@NPI (Czech Republic) at room temperature. Studied samples were placed in a vanadium container with diameter of 13 mm. Height of the neutron beam was adjusted for each sample individually. Neutron wavelength of 1.4618 Å was selected from white beam by mosaic copper monochromator. Diffraction patterns were collected between 4° and 144° of 2θ with a step of 0.08°. Structural refinements using full pattern fitting method were performed by FullProf software.[27] To determine microstructural effects of the sample instrument resolution function (IRF) describing instrument contribution to the resolution was used. IRF was determined by fitting of diffraction pattern of standard SiO_2 powder with the same instrument setup.

Surface area was measured by a sorption analyser Coulter SA 3100 (Backman Coulter). The samples were outgassed for 4 hours at 95 °C under high vacuum (VALUE) prior to the sorption experiments. The reason for such low temperature is to avoid degradation and further decomposition of oxygen functionalities, present mainly in CRG, on graphene. A TCD nitrogen cooled (77 K) detector was used for the evaluation of the results using a BET and Kelvin equations.

Results and discussion

Chemically reduced graphene (CRG) and thermally reduced graphene (TRG) were prepared and analysed by a large number of analytic techniques to determine the average number of graphene layers and crystallite size. These techniques included SEM, TEM, AFM, Raman spectroscopy, BET, XPS, X-ray diffraction and neutron diffraction methods. Analysis of the full diffraction patterns was used to calculate the essential parameters, such as interlayer spacing for a few layer graphene and in-plane average carbon-carbon atomic distances.

The morphology was investigated by SEM (**Figure 1**). The typical differences between CRG and TRG were observed. CRG has a "platelet" microstructure with just minor wrinkling of graphene sheet edges. TRG has a dissimilar microstructure, composed of "worm-like" expanded structures originating from the graphite oxide expansion caused by thermal shock followed by gas evolution. Highly wrinkled morphology indicates high concentration of structural defects. These materials exhibit a characteristic morphology observed by SEM, however, this gives only minor information about the number of layers and other structural properties.

CRG and TRG were also analysed by STEM (**Figure 2**). Similarly to SEM, highly wrinkled microstructure was observed on TRG. The main disadvantage of STEM is the fact that only a small area can be analysed. Moreover, samples have to be redispersed by ultrasonication before their positioning on the STEM grid. This procedure can reduce not only the size of graphene sheets but also the number of layers. Generally, microscopic techniques are not able to provide a general view on the microstructure since only a minor part of the sample is investigated.

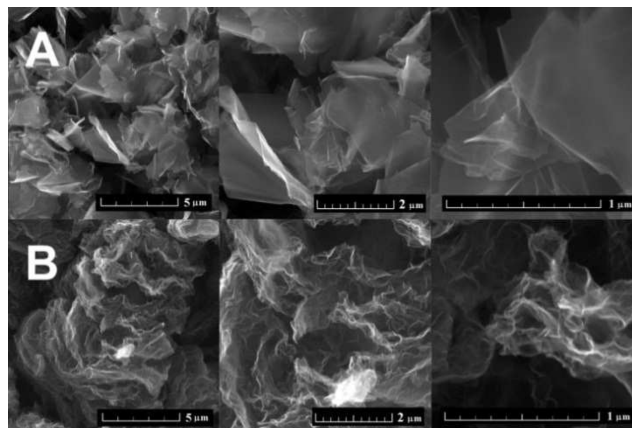

Fig. 1 The morphology of CRG (A) and TRG (B) obtained by SEM

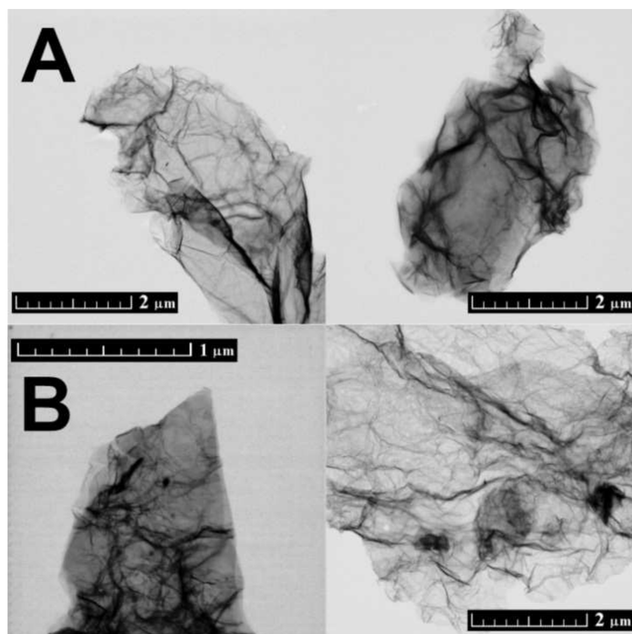

Fig. 2 The morphology of CRG (A) and TRG (B) obtained by STEM in bright field mode.

The comparable results to SEM and STEM were obtained by AFM microscopy. The AFM scan of TRG and CRG sample are shown in **Figure 3**. The AFM microscopy has similar limitations like TEM/STEM where only a limited number of graphene sheets can be investigated and sample is prepared for measurement by dropping of ultrasonicated solution. The desperation by ultrasonication led to the changes of the sample and further exfoliation and reduction of particle size. The wrinkled structure of reduced graphene can also bring about a misinterpretation in terms of the number of layers observed on the sample. This is clearly documented by the height profile of TRG sample for line 1 and line 2 in **Figure 3**. The line 1 gives a height of 2.4 nm corresponding to two-layer graphene. On the line 2 we can see a height of 3.7 nm for the same sheet. This discrepancy originates from the wrinkled rim of graphene sheet.

Nanoscale Accepted Manuscript

Elemental combustible analysis was used to determine the concentration of C, H and N in both graphene materials. The concentration of oxygen was obtained as a remainder to 100%. CRG revealed a lower degree of reduction and the concentration of C, O, H and N was 84.16 wt.%, 14.16 wt.%, 1.09 wt.% and 0.59 wt.%, respectively. TRG had a different composition, 93.16 wt.% of C, 5.86% of O, 0.87 wt.% of H and 0.11 wt.% of N. Nitrogen present in the samples originated from the synthesis of the starting material – graphite oxide, and it is also introduced into CRG by reduction with hydrazine.

Further characterization was performed by X-ray photoelectron spectroscopy to determine the degree of oxygen functionalities removal while survey spectra were used to calculate the C/O ratios. Only oxygen (O 1s at 532.5 eV) and carbon (C 1s at 284.5 eV) without any contamination were detected. (**Figure 4**). Based on the survey spectra, we calculated the C/O ratio 6.9 for CRG and 8.7 for TRG. Higher values of C/O ratio are typical for TRG as the high temperature treatment is accompanied by a decomposition of oxygen functionalities. The high resolution C 1s spectra were used to identify various remaining oxygen functionalities. (**Figure 4**). Deconvolution of the C 1s peak was carried out for the position of the C=C bonds at 284.5 eV, C–C/C-H bonds at 285.4 eV, C–O bond at 287.2 eV, C=O bond at 288.6 eV, O–C=O bond at 289.8 eV and π–π interactions at 290.5 eV. The obtained results are compiled in **Table 1**. To summarize the findings of chemical analysis, we can conclude that CRG and TRG exhibit almost the same composition, with the TRG sample having slightly higher degree of reduction.

Table 1. The results of C 1s peak deconvolution for CRG and TRG in %.

	C=C	C-C /C-H	C-O	C=O	O-C=O	$\pi-\pi^*$
CRG	48.8	28.7	8.6	2.4	3.3	8.3
TRG	49.8	18.7	12.8	4.3	3.1	11.3

Raman spectroscopy was employed to study the structure quality and crystallite size. The Raman spectra (**Figure 5**) showed two major bands located at 1580 cm^{-1} and 1340 cm^{-1}. The G band at 1580 cm^{-1} corresponds to the vibration of carbon in trigonal coordination (sp^2 hybridization) within graphene layer while the D band located at 1340 cm^{-1} is associated with defects in the hexagonal graphene framework and with sp^3 hybridized carbon atoms.[28] Small differences in the D/G ratios indicate different structural quality. The D/G ratios of peak maxima are 1.17 for CRG and 0.93 for TRG. The average crystallite size (L_a) of CRG and TRG was calculated according to the Eq. 1.[29]

$$L_a = 2.4 \times 10^{-10} \times \lambda_{laser}^{4} \times I_G / I_D \qquad \text{(Eq. 1)}$$

where λ_{laser} is the wavelength of the excitation laser in nanometres, and I_G and I_D are the intensities of the Raman *G* and *D* bands, respectively. The crystallite size obtained by this calculation is 16.4 nm and 20.7 nm for CRG and TRG, respectively. These values are slightly off when compared to data evaluated from neutron and X-ray diffractions that will be discussed later. The depth of information obtained by Raman

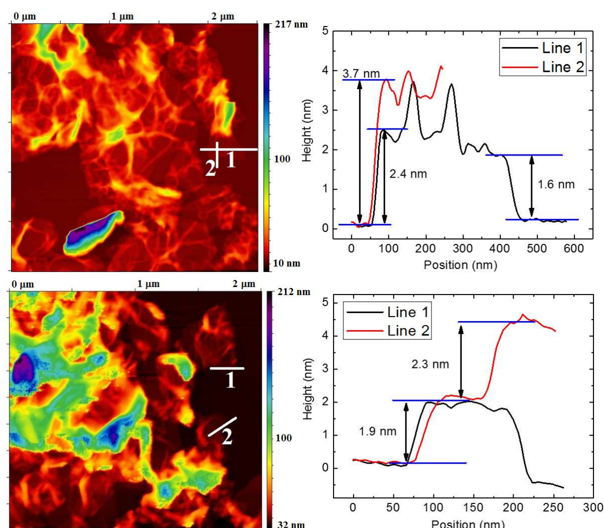

Fig. 3 AFM image of TRG (top) and CRG (bottom) sample and height profiles for two line scans.

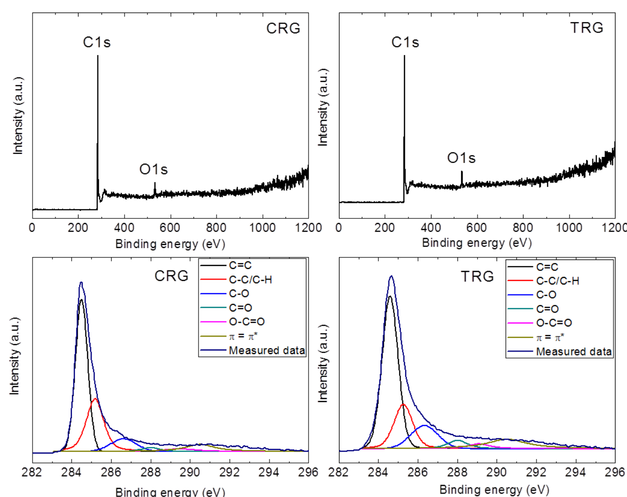

Fig. 4 XPS survey spectra (top) and high-resolution XPS spectra of C 1s signal (bottom) of CRG (right) and TRG (left).

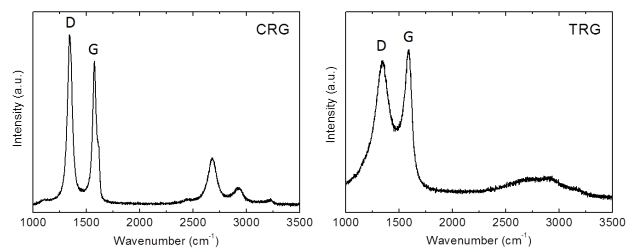

Fig. 5 Raman spectra of CRG and TRG samples.

spectroscopy originates from an area of several μm^2 (~hundreds of graphene sheets) which is further determined by laser focus and magnification of the microscope objective. On the other hand, crystallite size in graphene *a-b* plane obtained by Raman spectroscopy can be strongly influenced by other factors, such as concentration of remaining oxygen functionalities or structural defects. All these factors can influence the D/G ratio. In general, it is well-established that D/G ratio obtained by Raman spectroscopy is not representative for whole sample.[30]

The average number of graphene layers can be also obtained

Nanoscale Accepted Manuscript

This journal is © The Royal Society of Chemistry [year]

by sorption techniques. Theoretical surface of a single-layer graphene is supposed to be 2630 $m^2.g^{-1}$. The average number of layers was obtained by dividing the theoretical value of surface area by the surface area of the investigated samples. Adsorption isotherms for both TRG and CRG are shown in **Figure 6**. The surface areas 23.38 $m^2.g^{-1}$ and 384.58 $m^2.g^{-1}$ were found for of CRG and TRG, respectively. That gives the corresponding average number of layers 115.5 for CRG and 9.5 for TRG. On the one hand, this method disregards the edges of graphene flakes but, on the other hand, the size of graphene sheets observed by STEM indicates only minor ratio of graphene edges surface to the overall graphene area. The most surprising results were observed for CRG where the surface area corresponds to more than 100 layers, which is far from reality. This can be explained by stacking of graphene plates which exhibit only minimal wrinkling and strong interlayer interaction. We can conclude that this method is not suitable for graphene structure characterization and evaluation of the average number of graphene layers.

Finally, detailed diffraction study of graphene using neutron and X-ray radiation was performed with the intention to understand structural changes accompanying graphene formation. Pure graphite was also analysed for comparison. Advantage of using neutron diffraction in this particular case is that the structure form factor does not decrease with diffraction angle and, consequently, information from high Q range (diffraction vector: $Q = 4\pi\cdot\sin\theta/\lambda$) can be employed. Unfortunately, a larger amount of sample is necessary for neutron diffraction measurements.

Colour coded normalized neutron diffraction patterns of graphite, CRG and TRG are shown in **Figure 7**. It is evident that in comparison with graphite both graphene show broader reflections, especially those related to ***c*** axis. The integrated reflection intensity of graphenes decreases but the intensity at low angle (diffuse scattering) increases. This is due to the reduction of particle size and disruption of long range order. Comparing the neutron diffraction patterns we can conclude that CRG shows broader reflections 00*l* and those related to the ***c*** axis and narrower reflections associated with the ***ab*** plane (in hexagonal layer) compared to TRG, *i.e.* CRG is apparently composed of thinner but relatively large sheets whereas TRG has smaller but thicker hexagonal sheets.

To describe the reflection profile and extract the size effect from it an anisotropic size broadening model was applied. This model takes use of Scherrer formula rewritten as a linear combination of spherical harmonics contributions.[31] For the graphite structure (space group $P6_3/mmc$ (194)) with Laue class 6/mmm this spherical harmonics expansion involves five refinable parameters. The contribution of size broadening to the profile of particular *hkl* reflection is described by Eq. 2:[32]

$$SIZE_{\mathbf{h}}(\theta_{\mathbf{h}},\varphi_{\mathbf{h}}) = \sum_{lm\pm} C_{lm\pm} Y^{\pm}_{lm}(\theta_{\mathbf{h}},\varphi_{\mathbf{h}}) \qquad \text{(Eq.2)}$$

where index **h** represents the individual *hkl* reflection, θ and φ are spherical coordinates of the **h** vector (normal to *hkl* plane) in crystallographic coordinate system, *C* are refinable parameters and *Y* are symmetrized spherical harmonics basis functions. It can be shown that for the Laue class 6/mmm the basis set involves the following non-vanishing elements: Y^+_{00}, Y^+_{20}, Y^+_{40}, Y^+_{60} and Y^+_{66}.

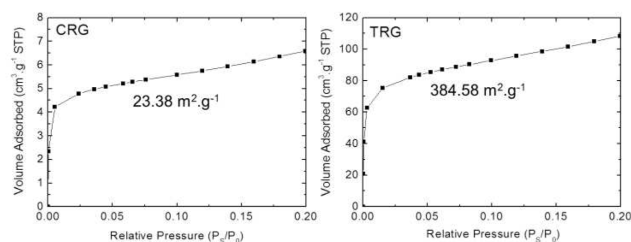

Fig. 6 Adsorption isotherms for CRG and TRG samples.

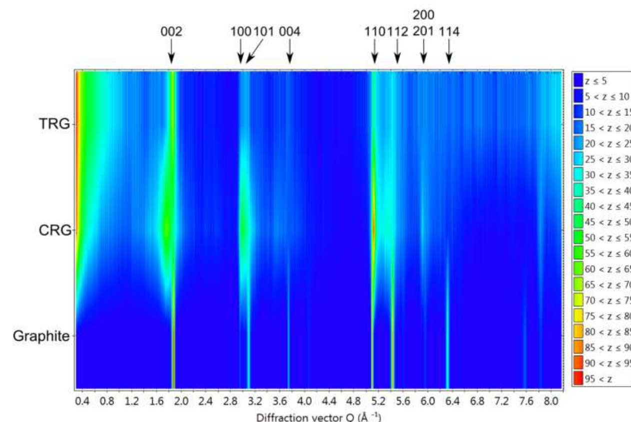

Fig. 7 Colour coded normalized neutron diffraction patterns of graphite, CRG and TRG. The z scale indicates the normalized intensity.

The same model for the size effect to the diffraction profile was also applied for the X-ray experiment. The measured and calculated neutron diffraction patterns using the described model for CRG and TRG and the reconstructed apparent particle shapes from refined *C* parameters (see Eq. 2) for both samples are shown in **Figure 8**. X-ray diffraction patterns are very similar. In **Figure 8** the comparison of normalized neutron and X-ray diffraction pattern of CRG and TRG is also shown manifesting the profound information gain acquired from the high Q values of neutron diffraction pattern.

The values of apparent sizes calculated form the selected reflections from neutron and X-ray diffraction patterns are given in the Table 2 for CRG and TRG. Carbon-carbon interatomic distances in and between hexagonal planes are listed in the Table 3. Taking into account the interplanar distances along with the apparent particle size we can estimate the corresponding number of hexagonal graphene layers stacked in <00*l*> direction. For CRG we found about 3 to 4 layers while for TRG 9 to 10 layers were typically identified. The results along *c* axis are similar for both neutron and X-ray diffraction. However, concerning the particle size along <*h*00> direction there are substantial differences between neutron and X-ray results. This can be due to the fact that neutron diffraction data bear more information for high Q reflections predominantly incident to *ab* plane, and can thus bring more accurate results (see Figure 8). Considering the results from neutron diffraction the apparent particle size in <*h*00> direction is about 250 Å for CRG and about 100 Å for TRG.

Nanoscale Accepted Manuscript

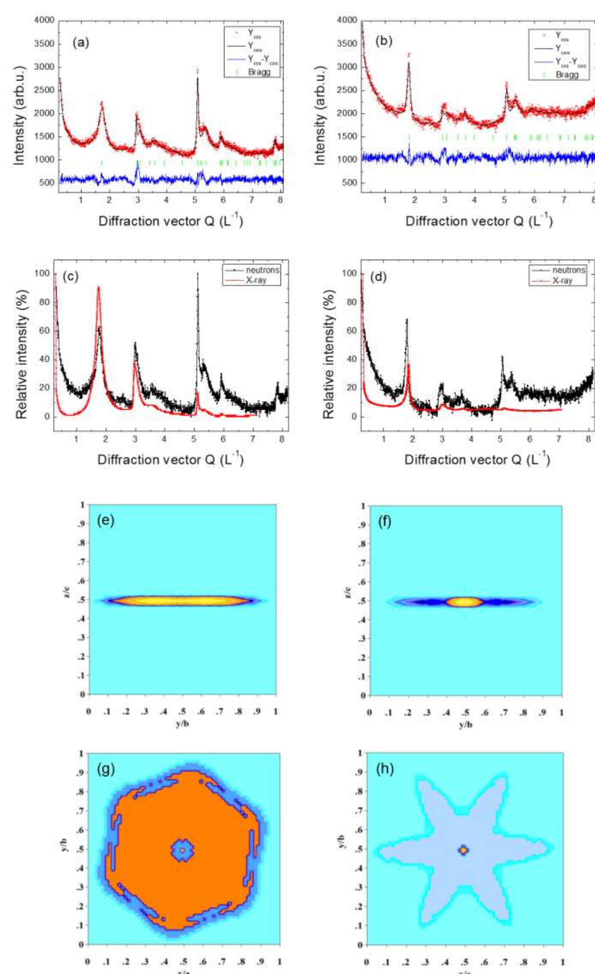

Fig.8 Measured and calculated neutron diffraction patterns for CRG (a) and TRG (b); comparison of neutron and X-ray diffraction patterns of CRG (c) and TRG (d). Reconstructed apparent size of the particles from neutron diffraction patterns displayed along <100> direction for the CRG (e) and TRG (f) and along <001> direction for the CRG (g) and TRG (h).

Table 2: Calculated values of apparent size along selected reflections for CRG and TRG sample obtained from neutron diffraction (ND) and X-ray diffraction (XRD).

Reflection	Apparent sizes of CRG (Å)		Apparent sizes of TRG (Å)	
	ND	XRD	ND	XRD
2	13.21	14.8	38.12	28.55
100	248.71	132.76	90.39	87.71
101	17.69	18.68	15.35	19.78
102	7.24	7.26	7.35	9.22
4	12.76	13.52	31.39	28.11
103	5.52	5.74	6.15	7.5
110	86.23	40.41	50.04	22.93
112	13.95	12.67	13.55	12.27
200	642.06	126.84	174.14	87.71

Table 3: Comparison of calculated interatomic (C-C) distances in and out of the hexagonal layer for graphite, CRG and TRG obtained from neutron and X-ray diffraction experiment.

	Neutron diffraction		
carbon-carbon (Å)	graphite	CRG	TRG
within hexagon layer	1.42507(2)	1.4266(2)	1.4333(5)
Between hexagon layers	3.3668(2)	3.638(3)	3.530(3)
	XRD		
carbon-carbon (Å)	graphite	CRG	TRG
within hexagon layer	1.4204(9)	1.4231(1)	1.4294(3)
between hexagon layers	3.3580(3)	3.6269(9)	3.4928(9)

The comparison of carbon-carbon distances in graphite and graphenes revealed a significant increase of the in-plane interatomic distance in TRG. Two effects are responsible for this increase, namely the formation of out of plane C-O bonds and the defects formation in graphene network. During the thermal and chemical reduction of graphite oxide, a large amount of functional groups is removed and the structure becomes restored. The reduction brought about a decrease of horizontal in-plane interatomic distances. Due to defects and remaining oxygen functionalities, the lattice parameters of CRG and TRG are not reaching those of graphite. The defects led to a formation of rings containing 5 or 7 carbon atoms and invoking the tilting of planar graphene sheets. This is the origin of graphene wrinkling observed on AFM and STEM pictures. As clearly seen from **Table 4** the presence of defects also results in an increase of average in-plane carbon-carbon atomic distances.

Table 4: Comparison of lateral size and number of layers calculated from different methods for CRG and TRG samples.

	CRG	TRG
Lateral size – Neutron diffraction (nm)	25	9
Lateral size – XRD (nm)	13	9
Lateral size – Raman spectroscopy (nm)	16.4	20.7
Number of layers – BET	115	9-10
Number of layers – Neutron diffraction	3-4	10
Number of layers – XRD	3-4	8

Finally, we compared the crystallite sizes and the number of layers obtained by various methods (**Table 4**). We can conclude that XRD and neutron diffraction provided the most valuable information on the number of layers. Differences in the number of layers obtained by BET originate from the restored interlayer interactions and subsequent reduction of surface area available for nitrogen absorption which is used as a measure of apparent surface area. In the case of TRG such effect does not exist due to

Nanoscale Accepted Manuscript

This journal is © The Royal Society of Chemistry [year]

higher concentration of defects which invoke substantial wrinkling of graphene sheets and inhibit the recovery of interlayer interactions. The differences in lateral size observed by Raman spectroscopy give different values compared to diffraction techniques. The crystallites size calculated from D/G ratio in Raman spectra is strongly influenced by other factors such as concentration of remaining oxygen functionalities which increase the intensity of D-band due to sp^3 hybridization of the involved carbon atoms.

Conclusions

We investigated the composition, grain size and the number of layers of graphene using microscopic techniques, such as SEM, TEM, AFM or Raman spectroscopy as well as bulk techniques as BET, X-ray diffraction and neutron diffraction. We demonstrated major advantages of neutron and X-ray diffraction for structural investigations of bulk amounts of graphene. Compared to various microscopic techniques, including SEM and STEM, diffraction methods can give overall information about graphene microstructure, namely the average number of layers and the lateral crystallite size. The data obtained from X-ray and neutron diffraction were also confronted with other techniques, BET adsorption analysis and Raman spectroscopy. Raman signal is usually influenced by the presence of remaining functional groups and defects in graphene structure. When compared to BET analysis, number of layers obtained by diffraction methods was in good agreement only for TRG. Significant differences found in the case of CRG are related to strong interactions between the graphene layers which considerably reduce the surface area available for nitrogen adsorption. We believe that X-ray and neutron diffraction are the most suitable methods for the evaluation of the number of graphene layers and crystallite size. Such methods do not require any sample preparation based on dispersing in solvents invoking changes in graphene structure. The use of proposed X-ray and neutron diffraction techniques is crucial for large scale (industrial) characterization of graphene materials as they are the only methods capable to provide accurate information on thickness and lateral size of graphene sheets on the bulk scales.

Acknowledgements

Z.S., P.Š., D.S. and O.J. thank for financial support from specific university research (MSMT No 20/2014). M.P. acknowledges Tier 2 grant (MOE2013-T2-1-056; ARC 35/13) from Ministry of Education, Singapore. P.B. acknowledge for support of infrastructure CANAM of the NPI ASCR Řež supported through MŠMT project No. LM2011019.

Notes and references

[a] Institute of Chemical Technology, Department of Inorganic Chemistry, 166 28 Prague 6, Czech Republic. E-mail: zdenek.sofer@vscht.cz; Fax: +420 22431-0422

[b] Nuclear Physics Institute of the ASCR, v. v. i., Husinec-Řež 130, 250 68 Řež, Czech Republic, E-mail:pberan@ujf.cas.cz

[c] Division of Chemistry & Biological Chemistry, School of Physical and Mathematical Sciences, Nanyang Technological University, Singapore, 637371, Singapore. E-mail:pumera@ntu.edu.sg; Fax: +65 6791-1961

1 A. K. Geim and K. S. Novoselov, *Nat. Mater.*, 2007, **6**, 183-191.
2 J.-H. Chen, C. Jang, S. Xiao, M. Ishigami and M. S. Fuhrer, *Nat. Nanotechnol.*, 2008, **3**, 206-209.
3 Y. Fan, L. Wang, J. Li, J. Li, S. Sun, F. Chen, L. Chen and W. Jiang, *Carbon*, 2010, **48**, 1743-1749.
4 K. S. Kim, Y. Zhao, H. Jang, S. Y. Lee, J. M. Kim, K. S. Kim, J. H. Ahn, P. Kim, J. Y. Choi and B. H. Hong, *Nature*, 2009, **457**, 706-710.
5 M. Pumera, A. Ambrosi, A. Bonanni, E. L. K. Chng and H. L. Poh, *TrAC Trends Anal. Chem.*, 2010, **29**, 954-965.
6 O. Jankovsky, P. Simek, D. Sedmidubsky, S. Huber, M. Pumera and Z. Sofer, *RSC Adv.*, 2014, **4**, 7418-7424.
7 O. Jankovsky, P. Simek, D. Sedmidubsky, S. Matejkova, Z. Janousek, F. Sembera, M. Pumera and Z. Sofer, *RSC Adv.*, 2014, **4**, 1378-1387.
8 S. Bae, H. Kim, Y. Lee, X. Xu, J. S. Park, Y. Zheng, J. Balakrishnan, T. Lei, H. Ri Kim, Y. I. Song, Y. J. Kim, K. S. Kim, B. Özyilmaz, J. H. Ahn, B. H. Hong and S. Iijima, *Nat. Nanotechnol.*, 2010, **5**, 574-578.
9 L. Staudenmaier, *Berichte Dtsch. Chem. Ges.* , 1898, **31**, 1481–1487.
10 W. Hummers and R. Offeman, *J. Am. Chem. Soc.*, 1958, **80**, 1339–1339.
11 B. C. Brodie, *Ann. Chim. Phys.*, 1860, **1860**, 466–472.
12 Z. Sofer, P. Simek and M. Pumera, *Phys. Chem. Chem. Phys.*, 2013, **15**, 9257-9264.
13 U. Hofmann and A. Frenzel, *Kolloid-Z.*, 1934, **68**, 149–151.
14 S. Park, J. An, J. R. Potts, A. Velamakanni, S. Murali and R. S. Ruoff, *Carbon*, 2011, **49**, 3019-3023.
15 C. K. Chua and M. Pumera, *J. Mater. Chem. A*, 2013, **1**, 1892-1898.
16 A. Ambrosi, C. K. Chua, A. Bonanni and M. Pumera, *Chem. Mater.*, 2012, **24**, 2292-2298.
17 C. K. Chua and M. Pumera, *Chem. Soc. Rev.*, 2014, **43**, 291-312.
18 X. Mei and J. Ouyang, *Carbon*, 2011, **49**, 5389-5397.
19 Z.-J. Fan, W. Kai, J. Yan, T. Wei, L.-J. Zhi, J. Feng, Y.-m. Ren, L.-P. Song and F. Wei, *ACS Nano*, 2010, **5**, 191-198.
20 Z. Sofer, O. Jankovský, P. Šimek, L. Soferová, D. Sedmidubský and M. Pumera, *Nanoscale*, 2014, **6**, 2153-2160.
21 J. C. Meyer, A. K. Geim, M. I. Katsnelson, K. S. Novoselov, T. J. Booth and S. Roth, *Nature*, 2007, **446**, 60-63.
22 M. J. McAllister, J.-L. Li, D. H. Adamson, H. C. Schniepp, A. A. Abdala, J. Liu, M. Herrera-Alonso, D. L. Milius, R. Car, R. K. Prud'homme and I. A. Aksay, *Chem. Mater.*, 2007, **19**, 4396-4404.
23 C. Gómez-Navarro, R. T. Weitz, A. M. Bittner, M. Scolari, A. Mews, M. Burghard and K. Kern, *Nano Lett.*, 2007, **7**, 3499-3503.
24 H. C. Schniepp, J.-L. Li, M. J. McAllister, H. Sai, M. Herrera-Alonso, D. H. Adamson, R. K. Prud'homme, R. Car, D. A. Saville and I. A. Aksay, *J. Phys.Chem. B*, 2006, **110**, 8535-8539.
25 G. Wang, J. Yang, J. Park, X. Gou, B. Wang, H. Liu and J. Yao, *J. Phys. Chem. C*, 2008, **112**, 8192-8195.
26 F. Banhart, J. Kotakoski and A. V. Krasheninnikov, *ACS Nano*, 2010, **5**, 26-41.
27 J. Rodríguez-Carvajal, *Phys. B: Condensed Matter,* 1993, **192**, 55-69.
28 M. S. Dresselhaus, A. Jorio, M. Hofmann, G. Dresselhaus and R. Saito, *Nano Lett.*, 2010, **10**, 751-758.
29 L. G. Cancado, K. Takai, T. Enoki, M. Endo, Y. A. Kim, H. Mizusaki, A. Jorio, L. N. Coelho, R. Magalhaes-Paniago and M. A. Pimenta, *Appl. Phys. Lett.*, 2006, **88**, 163106-163106-163103.
30 J. M. Englert, C. Dotzer, G. Yang, M. Schmid, C. Papp, J. M. Gottfried, H.-P. Steinrueck, E. Spiecker, F. Hauke and A. Hirsch, *Nature Chem.*, 2011, **3**, 279-286.
31 P. Scherrer, *Gött. Nachrichten Ges.* , 1918, **2**, 98–100.
32 M. Jarvinen, *J. Appl. Crystallogr.*, 1993, **26**, 525-531.

Nanoscale Accepted Manuscript